2012

Convective Flow Boiling of R-134a on Micro-Structured Aluminum Surfaces

Andrew D. Sommers
sommerad@muohio.edu

Kirk L. Yerkes

Convective Flow Boiling of R-134a on Micro-Structured Aluminum Surfaces

Andrew D. Sommers[1,*], Kirk L. Yerkes[2]

[1] Dept. of Mechanical and Manufacturing Engineering, Miami University, Oxford, OH 45056 USA
Phone: (513) 529-0718, Fax: (513) 529-0717, E-mail: sommerad@muohio.edu

[2] Propulsion Directorate, Air Force Research Laboratory, AFRL/RZP, WPAFB, OH 45433 USA
Phone: (937) 255-6186, Fax: (937) 656-4028, E-mail: kirk.yerkes@wpafb.af.mil

ABSTRACT

In this study, we have examined the convective flow boiling performance of R-134a on various micro-structured aluminum surfaces produced using advanced manufacturing techniques. More specifically, we have calculated the boiling heat transfer coefficient of R-134a on a bare aluminum surface and three micro-structurally enhanced surfaces. Two of these surfaces were produced using photolithography and reactive ion etching techniques, and the third surface was produced by means of laser-ablation.

Experiments were performed in a conventional two-phase, single-pass loop which allowed for heat transfer and pressure drop measurements over a range of inlet qualities with only small quality changes occurring in the test section. There was also optical access to the test specimen to permit flow visualization. To begin, both single-phase and two-phase flow experiments were performed on the bare aluminum surface to compare these baseline results with data found in the literature. Once baseline testing and validation were complete, the sample was exchanged and the three micro-structured surfaces were then each subsequently tested. The temperature and pressure of the refrigerant were measured at stations in the flow upstream and downstream of the test section, and the temperature of the test surface was measured using five T-type thermocouples in contact with the sample. The evaporation of the refrigerant was driven by thin ceramic heaters in contact with the underside of the test samples. The pressure, temperature, and quality within the test section were prescribed using an upstream heat exchanger, and the mass flow rate of the refrigerant was controlled using a magnetic gear pump and measured using a positive displacement flow meter. Experiments were performed for mass fluxes between 75 and 600 kg/m^{2}s and for heat fluxes between 5 and 25 kW/m^2.

1. INTRODUCTION

Structured and chemically coated surfaces have been studied for many years in an effort to better understand and enhance nucleate boiling from a heat transfer surface. Nucleate boiling as a physical process is well-known for its ability to remove high heat loads from a device at relatively low wall superheat temperatures. This ability to achieve these high heat removal rates inherently stems from the formation and transportation of the vapor bubbles and is believed to be due to three mechanisms: (1) thin film evaporation of the superheated liquid surrounding the growing bubble, (2) stripping of the thermal boundary layer at the wall by departing bubbles, and (3) the generation of turbulence in the liquid pool by escaping bubbles which produces a forced convection process. The first of these proposed mechanisms involves the transfer of heat via latent energy. The last two mechanisms primarily move the heat in the form of sensible energy.

Despite the proliferation of research on flow boiling and pool boiling from enhanced surfaces over the past decades and its clear potential for heat transfer enhancement, new methods for fabricating and analyzing surfaces have prompted ongoing research in the field. Some of these methods which have been used by the semi-conductor industry on model surfaces such as silicon and polymers (i.e. plasma etching, photolithography, etc.) have been applied far less to metallic surfaces such as those found in traditional heat transfer systems. In fact, very little research has been published where these techniques have been applied to polycrystalline aluminum and copper heat transfer surfaces. The application of these methods could potentially lead to significant enhancements in boiling heat transfer and improved thermal management. Thus, the continued investigation and fundamental study of new emerging novel enhanced surfaces is still needed.

* Assistant Professor, corresponding author

Surface enhancement technology can generally be classified into two categories—active techniques and passive techniques (i.e. those that require an external power supply and those that do not). An example of a passive technique is the micro-structuring of the surface. Several different methods have been used historically to create micro-structured surfaces including inscribing open grooves in the surface with a sharp pointed scribe (Bonilla et al., 1965), forming three-dimensional cavities by cold pressing conical cavities into the surface (Benjamin and Westwater, 1961), electroplating (Albertson, 1977), wet chemical etching (Muellejans, 1982), sintering metal particles or metal fibers onto the surface (Milton, 1968), spraying molten metal onto the surface (Grant and Kern, 1980; Cieslinski, 2000), and coating the surface with a particle-containing paint (You et al., 1998). Many researchers have also attempted to explain boiling heat transfer from such surfaces. One such study attributed the enhancement to primarily four things—extended surface area, capillary-assist in keeping the surface wetted, increased nucleation site density, and the effect that the cavity distribution has on vapor escape paths (Liter and Kaviany, 2001). Other excellent studies concerned with boiling on structured surfaces include Collier and Thome (1994), Rohsenow (1952), Forster and Zuber (1955), Bergles (1988), and Webb (1994).

Two methods not mentioned above are (1) laser etching, and (2) plasma etching—more specifically, reactive ion etching (RIE). Compared to wet chemical etching which inherently is isotropic, reactive ion etching allows for anisotropic etching of the underlying substrate. When coupled with photolithography, this method permits very complex geometries to be created on the surface. These surface structures could provide greater capillary-assist and facilitate the trapping of vapor in the cavity following bubble departure which would shorten the waiting period before new bubble formation. These surfaces can also be designed to have hydrophobic wetting behavior which tends to lessen the required superheat for nucleation at the surface. Laser etching is more cost effective than reactive ion etching and can still permit the creation of complex surface geometries; however, laser etching is not an anisotropic process. Thus, the sidewalls are not vertical like those produced by reactive ion etching. Because the underlying material is removed by ablation, the resulting microchannels are rounded, and the resulting surface contains significant nanoscale/microscale roughness.

The effect that surface wettability can have on nucleate boiling was first demonstrated by Bankoff (1957). The free energy of formation of a nucleus of radius *r* can be calculated from

$$\Delta G(r) = 4\pi r^2\sigma - \frac{4}{3}\pi r^3(P_v - P_l) \quad (1)$$

where σ is the surface tension of the liquid-vapor interface and $(P_v - P_l)$ is the pressure difference between the bubble vapor pressure and the pressure of the surrounding liquid. Bankoff (1957) was able to show that the $\Delta G(r)$ can be reduced by a factor φ such that

$$\varphi = \frac{(2+2\,cos\theta+cos\theta\,sin^2\theta)}{4} \quad (2)$$

where θ is the contact angle formed between the surface and the liquid. Thus, for a completely wetting surface, θ = 0° and $\varphi = 1$ and there is no reduction of the free energy of formation. For a completely non-wetting surface, however, θ = 180° and φ = 0 which indicates that no superheat of the surface should be necessary for nucleation to occur. Perhaps more importantly, this analysis suggests that a surface possessing non-wetting behavior should require less superheat than a wetting surface and therefore exhibit better boiling heat transfer performance. This method of fabrication (i.e. reactive ion etching) has already been applied to aluminum and has been shown to successfully increase the contact angle of water droplets placed on the surface by micro-syringe (see Fig. 1).

The special relevance that vapor generation has on the heat transfer from these proposed surfaces should also be mentioned. Recent bubble growth theory tends to separate the growth of bubbles into two distinct time periods—the initial growth stage and the final growth and departure stage as seen in Fig. 2 (Zhao et al., 2002). During the initial growth period, the emerging bubble is hemispherically shaped, and a wedge-shaped liquid microlayer exists below the bubble base. The evaporation of this microlayer liquid region promotes additional bubble growth and is extremely efficient at pulling away heat from the nucleating region. In contrast, the dry spot that extends out from the nucleation site is rather inefficient at removing heat and serves to reduce the microlayer. (For this reason, a hydrophobic surface should have a smaller dryout region and improved heat transfer.) Eventually, the final growth stage begins, and the bubble's center of mass begins to move upwards as the buoyancy force exceeds the inertial and surface tension forces acting on the bubble. During this period, the bubble shape changes from hemispherical to spherical, growth of the microlayer is limited, and most heat transfer occurs through the macrolayer. Thus, for a micro-structured surface to enhance heat transfer, it should contain many nucleation sites, facilitate liquid transfer to the microlayer region (to prevent dry-out), and assist in retaining vapor bubbles at the nucleation site longer.

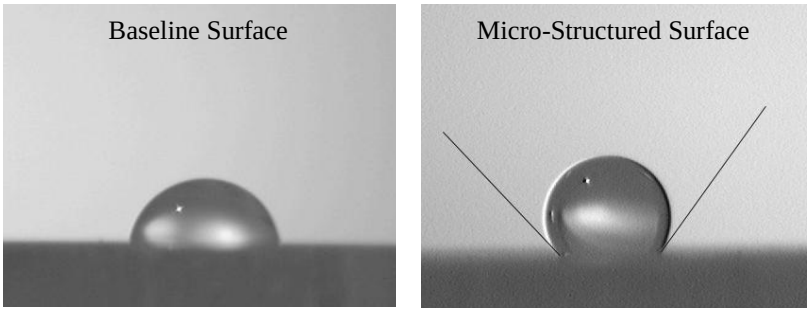

Figure 1: Image of a water droplet on a micro-structured aluminum surface and the impact of this surface structure on the contact angle

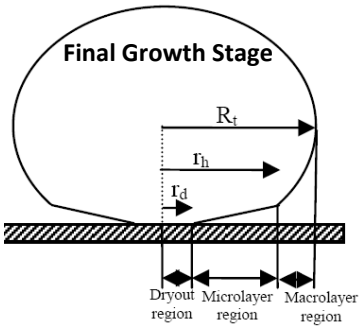

Figure 2: Final bubble growth stage (Zhao et al., 2002)

2. EXPERIMENTAL METHOD

2.1 Two-Phase Heat Transfer Flow Loop

The constructed loop (shown below in Fig. 3) which was designed to be operated in a pump-driven mode consisted of five major sections: thermal-conditioning, flow-conditioning, test section, condenser, and reservoir. Before reaching the evaporator test section, the refrigerant first passed through a thermal-conditioning section consisting of a subcooler and an electric preheater. The subcooler which was designed to cool the R-134a below the saturation state consisted of a ¾-inch ID copper pipe inserted into a copper block chilled by a circulating water jacket. A 30-inch long entrance region was used to condition the flow and ensure fully-developed turbulent flow conditions before reaching the test section, and the preheater was designed to control the quality of the entering refrigerant. An air-cooled condenser was used to return the refrigerant to the saturation state after leaving the test section, and a 1-liter reservoir was used to separate the two phases upstream of the pump inlet. The total charge of R-134a in the system was approximately 6.5 lbs.

Type-T thermocouple probes calibrated against an AFRL-traceable high-precision platinum RTD were used to measure the inlet and outlet temperatures of the R-134a and water in the test section, and four type-T thermocouples in good thermal contact with the underside of the aluminum plates were used to measure the wall surface temperature. Two more thermocouples were used to spot check the temperature of the phenolic material used to insulate the aluminum plates to check for heat loss. Following calibration, the uncertainty associated with these thermocouples was determined to be ±0.04 °C with 95% confidence. Two OMEGA PX409 high accuracy pressure transducers with an uncertainty of ± 0.12 psi are used to measure the pressure drop across the test section. The volumetric flow rate of the fluid can be varied from 0.25 GPM to 2.0 GPM and measured using an oval gear, positive displacement flow meter (OMEGA) with an uncertainty of ± 0.5% of the reading.

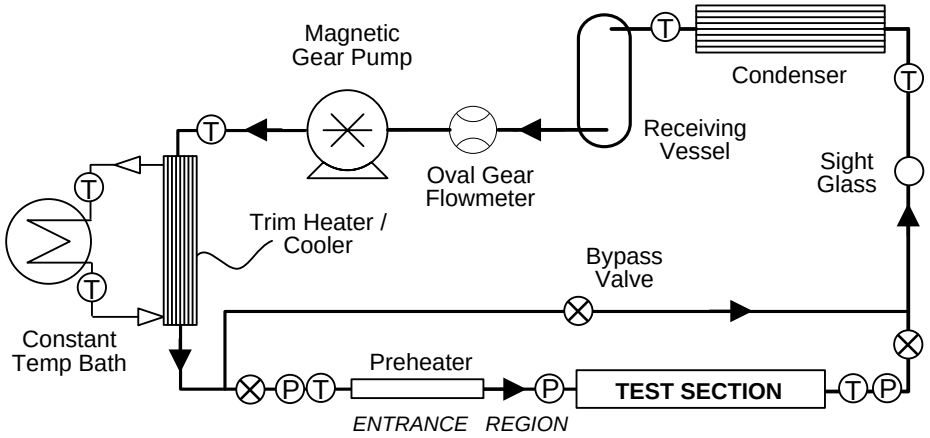

Figure 3: Schematic of the two-phase convective flow boiling test loop

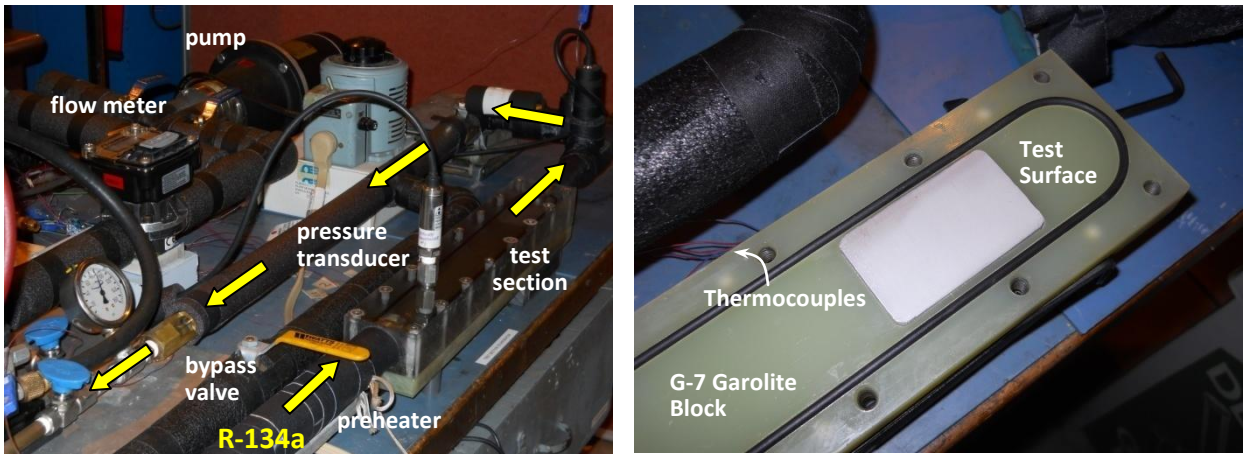

Figure 4: Pictures of the constructed flow boiling test loop

The test section consists of a 2.5-inch long aluminum plate embedded in a clear acrylic block for flow visualization (see Fig. 4). Four thick film heaters (0.675" x 0.499" x 0.030") supplied by Mini-Systems, Inc. with a nominal resistance of 2.3 Ω each are used for the nucleate boiling. A shunt resistor will be used to measure the actual current flow and determine the supplied heat input. Heat rates from 5 to 100W are planned by varying the supply voltage to the four heaters. For an input voltage of only 6 VDC, however, these heaters can collectively provide approx. 60W of heat. This equates to a heat flux of approximately 25 W/cm^2. Silicone grease was used to ensure good thermal contact between the heaters and the aluminum plate, and the heaters were embedded in a G-7 Garolite block (i.e. phenolic material) to minimize heat losses to the surroundings. Fiberfrax high-temperature insulation was used to insulate the electric preheater located immediately upstream of the test section. Significant time was devoted to ensuring that the loop was free of leaks. The main loop was eventually evacuated and charged with refrigerant.

2.2 Fabrication of Test Surfaces

Four different surface geometries were prepared for evaluation in the test section—(1) baseline, (2) micro-channels perpendicular to the flow, (3) square micro-posts, and (4) laser etched micro-channels perpendicular to the flow (see Table 1). The test surfaces were constructed from aluminum alloy 1100 with a mill finish and were approximately 38.1 mm × 61.9 mm × 3.175 mm in size. Standard photolithographic practices were used to prepare the plates for etching (see Fig. 5). First, a photoresist was spin-coated onto the surface using a spinner and then soft baked to prevent mask sticking. A Quintel Q7000 IR Backside Mask Aligner (or equivalent) was then used to align the mask over the substrate and expose the photoresist to UV light. Development was by immersion and agitation in a beaker. Following development, the samples were post-baked to completely harden the masking layer before transferring them to a PlasmaTherm Inductively Coupled Plasma Reactive Ion Etcher (ICP RIE) for dry chemical etching. After etching, the samples were rinsed with copious amounts of acetone and gently brushed with a swab to remove the photoresist layer. Finally, an ashing step was performed to remove any remaining organic material on the surface by means of an oxygen plasma. Unlike the other samples, the micro-channels on Surface 4 were laser etched using a Trumpf laser system. SEM images of all four surfaces can be seen in Fig. 6.

2.3 Data Reduction Methodology

The following data reduction procedure was employed to determine the inlet and outlet refrigerant quality and steady-state boiling heat transfer coefficient, h_{tp}, using temperature and pressure data recorded from the test section during two-phase heat transfer experiments. A commercial software program (Engineering Equation Solver, EES) was used to determine all thermodynamic properties of the pure refrigerant used in these experiments which was R-134a. (Note: No oil was used in the course of these experiments.) The heat transfer to the test surface in the test section was applied using four thin-film ceramic heaters arranged under the surface in two rows. To accurately determine the amount of applied heat, the voltage and current were measured for two of the heaters. In this way, the total heat transfer to the refrigerant was found using Joule's law such that

$$Q_{electric} = 2(V_1 I_1) + 2(V_2 I_2) \quad (3)$$

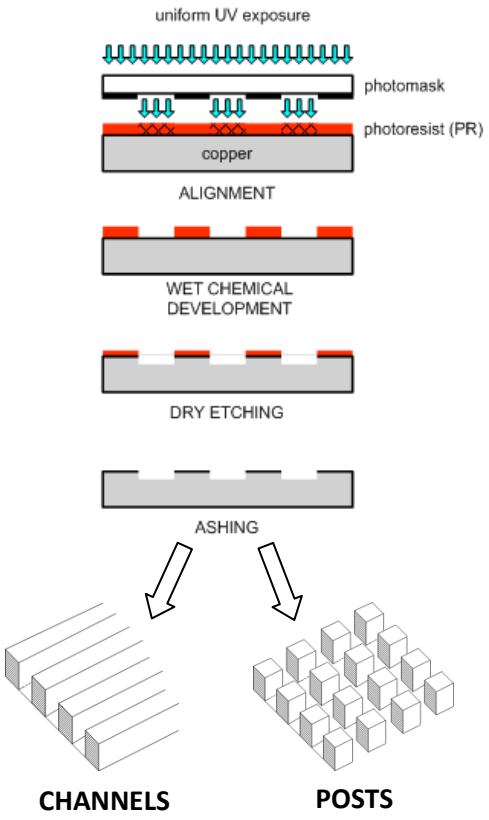

Figure 5: Photolithographic procedure used to prepare Surfaces 1-3

Table 1: Matrix of aluminum test surfaces

No.	Material	Geometry	Width / Depth	Orientation	Method
1	Al	*none*	*none*	--	--
2	Al	channel	17.7μm / 12.2μm†	⊥ to flow	*RIE*
3	Al	post	17.7μm / 12.2μm†	*n/a*	*RIE*
4	Al	channel	100 μm / 10 μm*	⊥ to flow	*laser*

NOTE: † Channel spacing approx. 12 μm; * Channel spacing approx. 25 μm

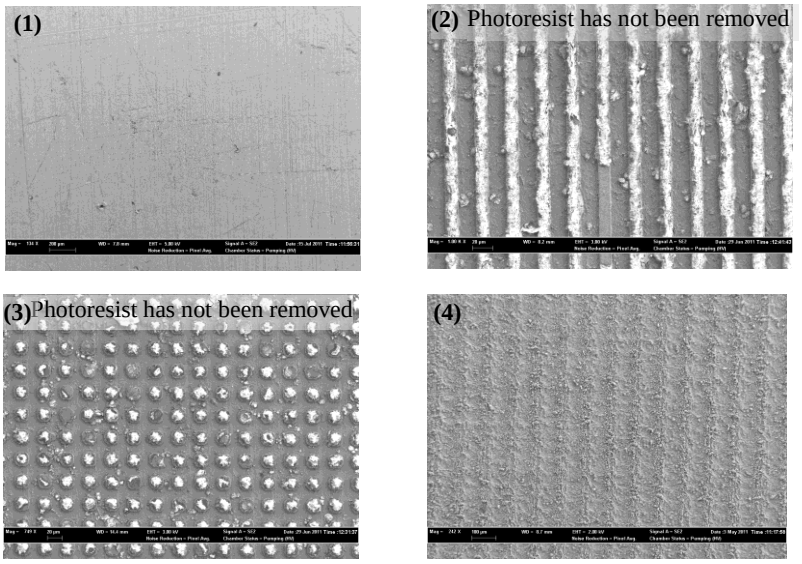

Figure 6: SEM images of prepared test surfaces— (1) baseline, (2) micro-channels, (3) micro posts, and (4) laser-etched micro channels

(Note: Measurement differences between the two heaters never exceeded 9%; during baseline testing, the average difference was only 5.4% for n = 44.) Once the heat input to the test surface was known, the average two-phase boiling heat transfer coefficient, h_{tp}, could be determined using

$$\bar{h}_{tp} = \frac{Q_{electric}}{\left[A(T_{wall,avg} - T_{r,avg}) - \frac{Q_{electric} t_{plate}}{k}\right]} \tag{4}$$

since

$$Q_{electric} = (T_{wall,avg} - T_{r,avg})\left[\frac{1}{\bar{h}_{tp} A} + \frac{t_{plate}}{kA}\right]^{-1} \tag{5}$$

where in this equation k is the thermal conductivity of the test surface (aluminum 1100); A is the test plate surface area; t_{plate} is the thickness of the plate; $T_{wall,avg}$ is the average surface temperature of the plate averaged using at least four thermocouple readings from the underside of the plate; and $T_{r,avg}$ is the saturation temperature of the refrigerant in the test section which was evaluated using the pressure P_{avg} where

$$P_{avg} = (P_{inlet} + P_{outlet}) / 2 \tag{6}$$

The refrigerant vapor quality at the inlet of the test section (i.e. x_{inlet}) was determined from the measured pressure (i.e. P_{inlet}) and the enthalpy as given by:

$$i_{inlet} = i_{sub} + Q_{preheat} / \dot{m}_r \tag{7}$$

where $Q_{preheat}$ is the heat transfer rate into the refrigerant from an electric preheater, i_{sub} is the enthalpy of subcooled R134a determined using the measured pressure and temperature before the preheater, and $\dot{m}_r$ is the mass flow rate of the refrigerant. In a similar manner, the refrigerant quality at the exit of the test section (i.e. x_{outlet}) was determined from the measured pressure (i.e. P_{exit}) and exit enthalpy given by:

$$i_{exit} = i_{inlet} + Q_{electric} / \dot{m}_r \tag{8}$$

where $Q_{electric}$ is the heat transfer rate into the refrigerant from Eq. (3) and i_{inlet} is the enthalpy of the R134a at the inlet of the test section as determined using Eq. (7). In this study, experiments were conducted such that changes in the refrigerant vapor quality within the test section were always less than 1.5% with the average quality change being only 0.4%. In this way, the calculation of a true quasi-local, average heat transfer coefficient, h_{tp}, was ensured.

Two published correlations were used to validate and compare with the baseline and enhanced test data. Equation (9) which was suggested by Jung et al. (1989) for both pure refrigerants and azeotropes is given by

$$h_{tp,Jung} = N h_{SA} + F_p h_{lo} \tag{9a}$$

where

$$N = 4048 X_{tt}^{1.22} Bo^{1.13} \tag{9b}$$

$$h_{SA} = 207 \frac{k_l}{bd} \left(\frac{q\, bd}{k_l T_{sat}} \right)^{0.745} \left(\frac{\rho_v}{\rho_l} \right)^{0.581} Pr_l^{0.533} \tag{9c}$$

$$bd = 0.0146 \beta [2\sigma / (g(\rho_l - \rho_v))]^{0.5} \quad \text{where } \beta = 35° \tag{9d}$$

$$F_p = 2.37 \left(0.29 + \frac{1}{X_{tt}} \right)^{0.85} \tag{9e}$$

$$X_{tt} = \left(\frac{1-x}{x} \right)^{0.9} \left(\frac{\rho_v}{\rho_l} \right)^{0.5} \left(\frac{\mu_l}{\mu_v} \right)^{0.1} \tag{9f}$$

Properties with the subscript *l* refer to the liquid phase and *v* refers to the vapor phase. The correlation by Kandlikar (1990) which was developed to fit a large range of flow boiling heat transfer data in vertical and horizontal tubes was also used as shown in Eq. (10) where:

$$h_{tp,Kandlikar} = maximum\ of \begin{cases} h_{NBD} \\ h_{CBD} \end{cases} \tag{10a}$$

$$h_{NBD} = 0.6683 \left(\frac{\rho_l}{\rho_v} \right)^{0.1} x^{0.16} (1-x)^{0.64} f_2(Fr_{lo}) h_{lo} + 1058.0 Bo^{0.7} F_K (1-x)^{0.8} h_{lo} \tag{10b}$$

$$h_{CBD} = 1.1360 \left(\frac{\rho_l}{\rho_v} \right)^{0.45} x^{0.72} (1-x)^{0.08} f_2(Fr_{lo}) h_{lo} + 667.2 Bo^{0.7} F_K (1-x)^{0.8} h_{lo} \tag{10c}$$

where h_{lo} is the single-phase heat transfer coefficient for the liquid phase flowing alone and f_2 is a function that depends on the Froude number. Table 2 summarizes the range in heat flux, mass flux, vapor quality, and saturation temperature achieved within the test section during baseline and enhanced surface testing. The resulting uncertainty of the reported boiling heat transfer coefficients was calculated and found to be 9-13% (using EES).

Table 2: Range of experimental test conditions

Heat Flux, q (kW/m^2)	Mass Flux, G (kg/m^{2}s)	Average Vapor Quality, x (%)	Saturation Temp, T_{sat} (°C)
1.4 – 25.2	60 - 590*	1.1 – 17.6†	20.5 – 27.0

* 300 – 590 kg/m^{2}s (typical); † 3.0 – 6.8 (typical)

3. RESULTS AND DISCUSSION

3.1 Baseline Data Validation

More than forty experiments were first conducted on the baseline surface (Surface 1) at different test conditions, and the resulting data are plotted on the Baker (1954) flow regime map developed for horizontal two-phase flow in tubes. As seen in Fig. 7, most test data were shown to fall within the slug flow regime which is commonly observed in air-conditioning applications. This is also consistent with the flow maps proposed by Sato et al. (1972) and others. The average vapor quality in the test section was typically below 0.20. Thus, as predicted by these flow maps, most of the data points were within the slug flow regime. These predicted flow patterns are also in good agreement with direct observations inside the transparent test section.

Next, the boiling heat transfer coefficient for the baseline surface acquired from the flow loop was compared to results predicted by the Jung et al. (1989) correlation as shown in Fig. 8. A certain amount of discrepancy was expected in this comparison because our flow loop and operating conditions were not exactly the same as those used by other groups. For example, the Jung et al. correlation (1989) over-predicted the experimental *h* value for eight data points as seen in Fig. 8. In each case, however, these larger deviations coincided with low experimental vapor qualities— something predicted by Jung et al. (1989) for low qualities. (Note: The average test section quality is superimposed by these data points in Fig. 8). It is also well-known that the two-phase heat transfer coefficient is affected by the saturation temperature, mass flux of the refrigerant, and the applied surface heat flux. This precluded the use of other well-known correlations such as Wattelet et al. (1991) and Panek et al. (1992). For example, Wattelet et al. (1991) gathered their data at T_{sat} = 4.4°C and x_{in} = 0.2 in all cases, while Panek et al. (1992) had a saturation temperature of 5°C. Even though the comparison is a bit loose, the general agreement of our data with a published correlation still validates our overall experimental methodology and approach.

3.2 Evaporative Heat Transfer Data on Enhanced Surfaces

Experiments were then performed on the topographically-modified, enhanced surfaces (i.e. Surfaces 2-4) under the same range of test conditions to permit comparisons to be made with the baseline surface. The results of these tests are shown in Figs. 9 and 10. Figure 9 shows the convective boiling heat transfer coefficient for Surfaces 2 and 3 as compared with the baseline surface (i.e. Surface 1), and Figure 10 shows the applied heat flux versus the wall superheat for these surfaces. A few observations can be made. First, both of the etched surfaces exhibited improved heat transfer performance as compared to the baseline surface. This was manifest in higher heat transfer coefficients (see Fig. 9) and reduced wall superheat (see Fig. 10). For example, for an applied heat flux of 10 kW/m^2, Surface 2 exhibited approximately a 35% increase in the heat transfer coefficient relative to the baseline aluminum surface.

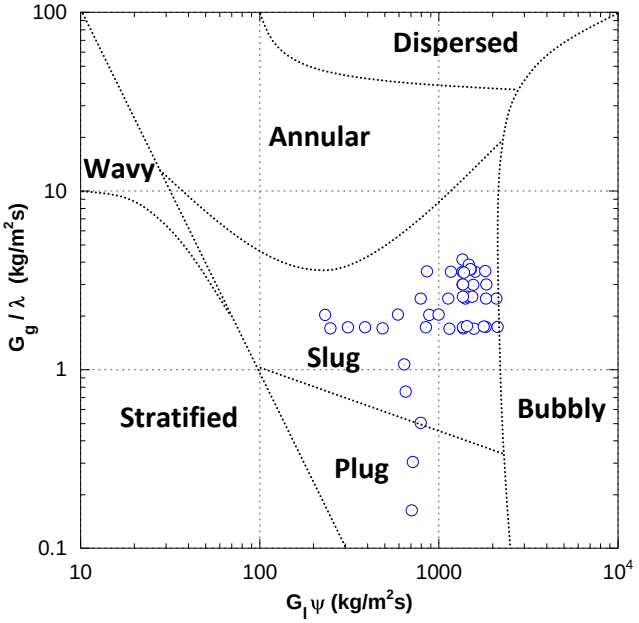

Figure 7: Flow pattern map (Baker, 1954)

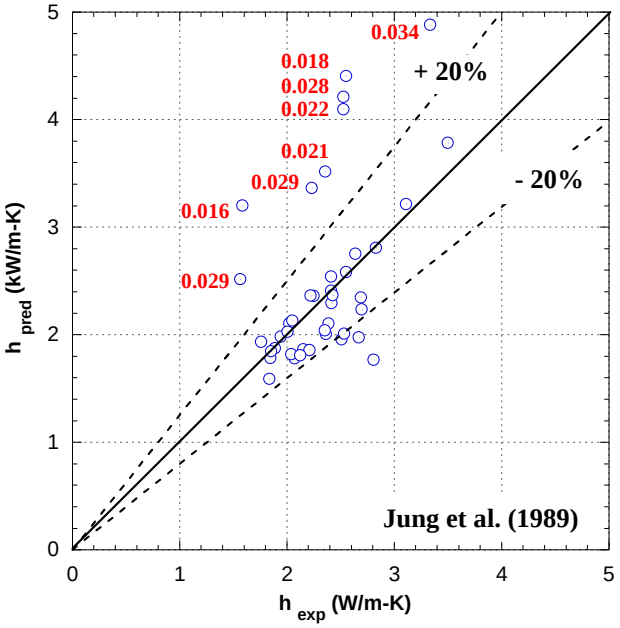

Figure 8: Comparison with Jung et al. (1989) model with vapor quality superimposed for cases of poor prediction

Second, no statistical differences were observed between Surfaces 2 and 3. (i.e. Both of the etched surfaces exhibited similar heat transfer performance as compared to one another.) This suggests that the increase in surface area (and thus nucleation sites) associated with the micro-post geometry (Surface 3) did not play a significant role here. It should be noted however that the surface wettability was similar for both of these samples. Thus, this may partially explain the similar performance that was realized for both of these surfaces. Third and finally, the data curves associated with the enhanced surfaces were observed to shift to the left on the q'' versus $T_w - T_{sat}$ plot shown in Fig. 10. This is consistent with the increased hydrophobicity of these surfaces (as compared to the baseline) which is known to shift this curve to the left. This is because if the liquid does not readily wet the surface, vapor (and/or air) will be trapped in some of the surface cavities when the surface is immersed in the liquid. Due to the abundance of these vapor-filled cavities, vaporization is thus initiated more rapidly when the surface temperature begins to exceed the saturation temperature. Rougher surfaces are also generally expected to provide a higher heat flux for a given wall superheat because of the higher density of potential nucleation sites. Surfaces 2 and 3 satisfy both of these criteria, namely— (i) they are *rougher* than Surface 1, and (ii) they are more *hydrophobic* than Surface 1. It is also worth noting that this increase in hydrophobicity was simply the result of modifying the surface topography. No surface coatings were used here.

The experimental heat transfer coefficients measured on Surfaces 2 and 3 were also compared to the predicted values using the well-established Kandlikar (1990) correlation as shown in Fig. 11. Excellent agreement was observed for both surfaces which further supports the accuracy of these data as well as our overall experimental methodology and approach. The average error was found to be 5.7% (n = 33). Next, the heat transfer coefficient for Surface 4 was plotted alongside the other surfaces. As shown in Fig. 12, this surface exhibited the greatest enhancement over the baseline surface. An increase in h of 94% was observed for a heat flux of approximately 12 kW/m^2. Compared to Surfaces 2 and 3, the laser-etched surface also consistently exhibited a larger heat transfer coefficient than either of these two surfaces. For applied heat fluxes of 12.2 kW/m^2, 15.6 kW/m^2, and 18.8 kW/m^2, the heat transfer coefficient on Surface 4 was 44%, 33%, and 37% higher than Surface 2, respectively. While the experimental range available for comparison is limited, the results are compelling. So how do these surfaces compare to existing enhanced surface designs? In Fig. 13, boiling heat transfer data for R-22 at T_{sat} = 4.4°C on various commercially available surfaces are shown. While care should be taken in drawing conclusions, the percentage increase in h over the baseline surface is comparable to that seen here. Furthermore, because the microstructure of Surface 4 is geometrically less complex and laser etching is amenable to mass manufacturing, the costs associated with producing such surfaces should compete favorably with these enhanced surfaces.

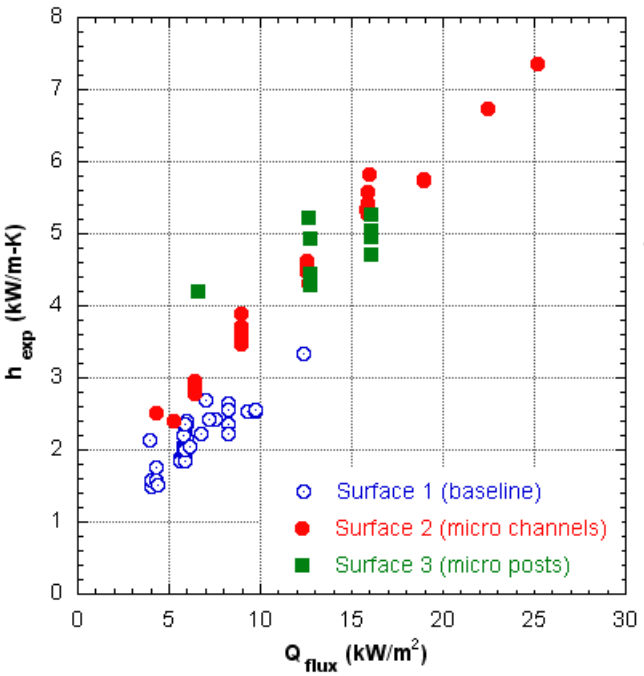

Figure 9: Experimental heat transfer coefficient versus applied heat flux for Surfaces 1, 2, and 3

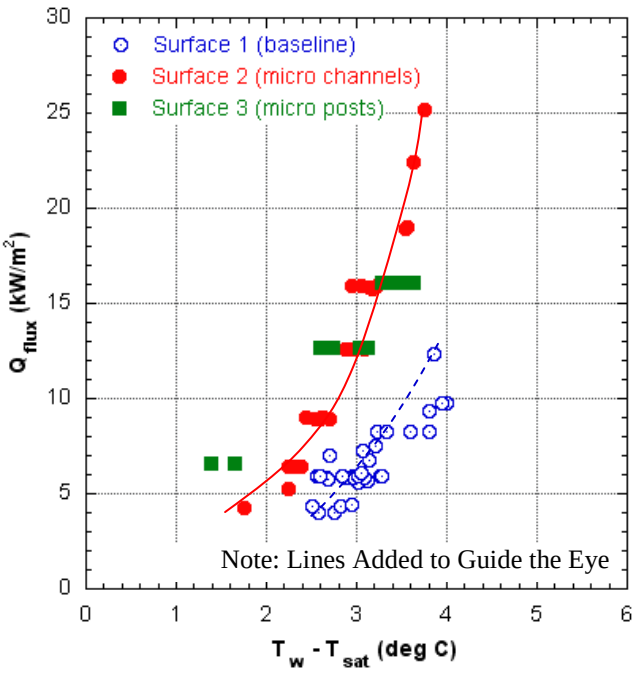

Figure 10: Applied heat flux versus wall superheat for Surfaces 1, 2, and 3

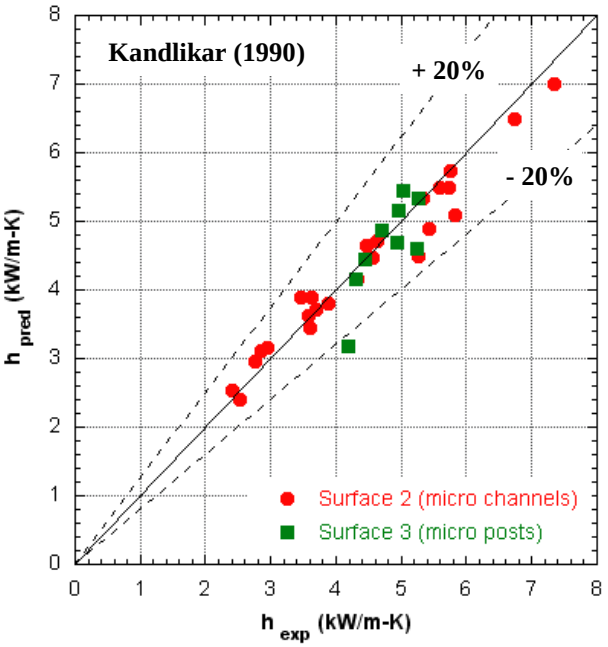

Figure 11: Comparison of our experimental data with the Kandlikar (1990) correlation shows excellent agreement

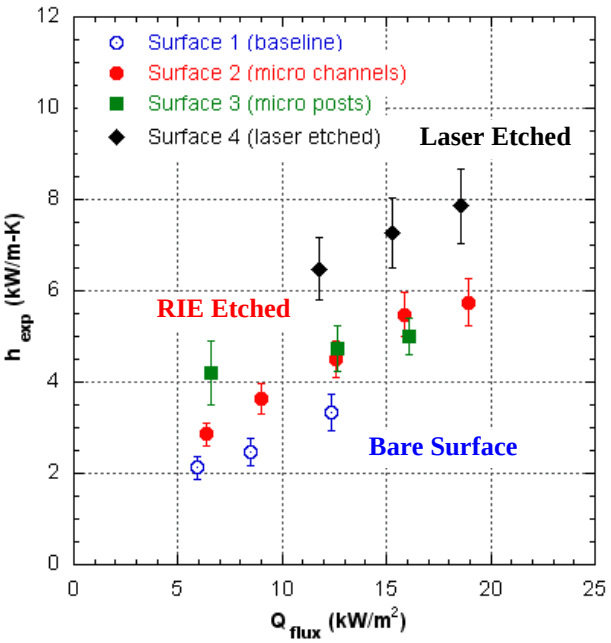

Figure 12: Comparison of Surface 4 versus the other surfaces reveals that it performed the best

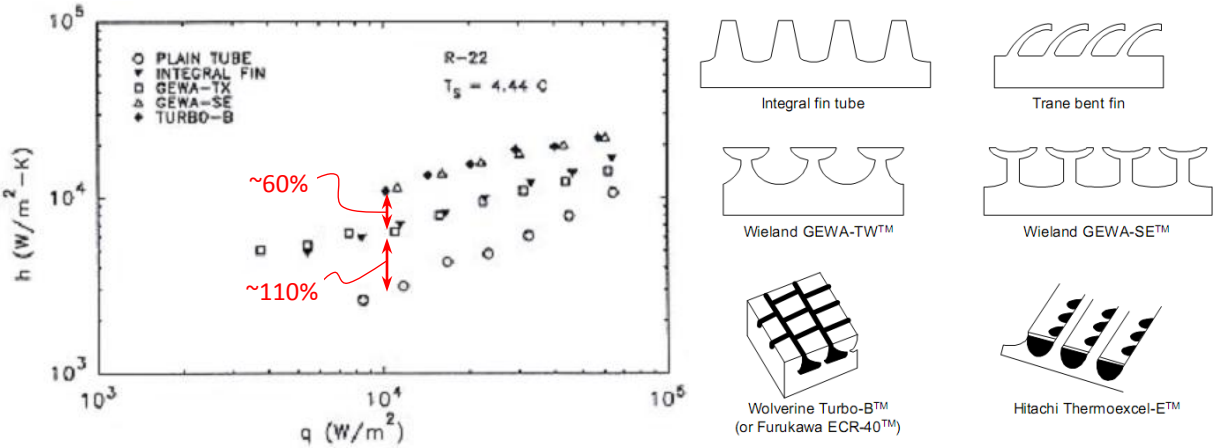

Figure 13: Heat transfer data for R-22 on commercially available enhanced surfaces (Webb, 1994)

4. CONCLUSIONS

The convective flow boiling heat transfer performance of R-134a on various micro-structured aluminum surfaces produced using advanced manufacturing techniques has been explored. Surfaces produced using photolithography and reactive ion etching techniques (i.e. Surfaces 2 and 3) showed a 35-48% increase in the boiling heat transfer coefficient over the baseline bare aluminum surface (i.e. Surface 1). One surface contained parallel microchannels aligned perpendicular to the flow, and the other surface contained square micro posts nominally 15 μm x 15 μm in size. A third enhanced surface was also tested which was produced by means of laser-ablation and contained parallel microchannels (nominally 100 μm wide) also aligned perpendicular to the flow. This surface (i.e. Surface 4) exhibited a 90-100% increase in the boiling heat transfer coefficient over the baseline surface and more than a 30% increase over the other enhanced surfaces. These observed enhancements were also reflected in lower overall required wall superheats. It is believed that the proposed micro-structure of these surfaces not only provided numerous additional sites for nucleation to occur (due to the localized roughness of the surface), but also helped keep these sites wetted due to the capillary assist provided by the channels/posts. Although the experimental range in this study was a bit limited, the results are nonetheless compelling and should warrant further investigation.

NOMENCLATURE

A	Heat transfer area	(m^2)
Bo	Boiling number	
Co	Convection number	
F_K	Fluid-dependent parameter	
Fr	Froude number	
G	Mass flux	(kg/m^2-s)
h	Heat transfer coefficient	(W/m^2K)
i	Enthalpy	(J/kg)
k	Thermal conductivity	(W/(m-K))
Pr	Prandtl number, $c_p\mu/k$	
q	Heat flux	(kW/m^2)
t	Thickness	(m)
V	Voltage	(V)
x	Vapor quality	
X	Martinelli parameter	

Greek Symbols

μ	Dynamic viscosity (Pa·s)
ρ	Density (kg/m^3)

Subscripts

lo	All-liquid
r	Refrigerant
sat	Saturation
tp	Two-phase
w	Wall

REFERENCES

Albertson, C.E., 1977, Boiling heat transfer surface and method. US Patent No. 4,018,264.

Baker, O., 1954, Simultaneous flow of oil and gas, *J. Oil and Gas* 53, pp. 85–195.

Bankoff, S.G., 1957, Ebullition from solid surfaces in the absence of a pre-existing gaseous phase. *ASME Transactions*, vol. 79, p. 735.

Benjamin, J.E., and Westwater, J.W., 1961, Bubble growth in nucleate boiling of a binary mixture, *International Developments in Heat Transfer*, ASME, New York, pp. 212-218.

Bergles, A.E., 1988, Some perspectives on enhanced heat transfer: Second-generation heat transfer technology. *Journal of Heat Transfer*, ASME, vol. 110, pp. 1082-1096.

Bonilla, C.F., Grady, J. J., Avery, G.W., 1965, Pool boiling heat transfer from grooved surfaces. *Chem. Eng. Prog. Supp. Ser.*, vol. 61, no. 57, pp. 280-288.

Cieslinski, J.T., 2000, Nucleate pool boiling on porous metallic coatings. *Proceedings of the ASME-ZSITS International Thermal Sciences Seminar,* Bled, Slovenia, June 11-14.

Collier, J.G. and Thome, J.R., 1994, Convective Boiling and Condensation, *Oxford Science Pub.*, 3rd ed.

Forster, H.K. and Zuber, N., 1955, Bubble dynamics and boiling heat transfer. *AIChE Journal*, vol. 1, p. 532

Grant, A.C., Kern, J.W., 1980, Thermospray method for production of aluminum porous boiling surfaces. US Patent No. 4,232,056.

Jung, D.S., McLinden, M., Radermacher, R., Didion, D., 1989, A Study of Flow Boiling Heat Transfer with Refrigerant Mixtures, *Int. J. Heat Mass Transfer* 32(9), pp. 1751-1764.

Kandlikar, S. G., 1990. A general correlation for saturated two-phase flow boiling heat transfer inside horizontal and vertical tubes. *J. Heat Transfer* 112, pp. 219-228.

Liter, S.G., Kaviany M., 2001, CHF enhancement by modulated porous layer coating: theory and experiment. *Int. J. Heat Mass Transfer*, 44(22), pp. 4287-4311.

Milton, R.M., 1968, Heat exchange system. US Patent No. 3,384,154.

Muellejans H., 1982, Process for the preparation of a surface of a metal wall for the transfer of heat. US Patent No. 4,360,058.

Panek, J.S., Chato, J.C., Jabardo, J.M.S., de Souza, A.L., Wattelet, J.P., 1992, Evaporation heat transfer and pressure drop in ozone-safe refrigerants and refrigerant-oil mixtures, *ACRC TR-11*, *Air Conditioning and Refrigeration Center*, University of Illinois at Urbana-Champaign.

Rohsenow, W.M., 1952, A method of correlating heat transfer data for surface boiling of liquids. *ASME Transactions*, vol. 74, pp. 969-976.

Sato, T., Minamiyama, T., Yanai, M., Tokura, T., 1972, Study of heat transfer in boiling two-phase channel flow – Part 1: Flow patterns in a boiling channel, *Heat Transfer Japanese Research*, vol. 1, no. 1, pp. 1-14.

Wattelet, J. P., Chato, J.C, Souza, A.L, Christoffersen, B.R., 1991, Evaporative characteristics of R-134a, MP-39, and R-12 at low mass fluxes, *ACRC TR-35*, *Air Conditioning and Refrigeration Center*, University of Illinois at Urbana-Champaign.

Webb, R.L., 1994, *Principles of Enhanced Heat Transfer*. John Wiley and Sons, Inc.

You, S.M., O'Connor, J.P., 1998, Boiling enhancement coating. US Patent No. 5,814,392.

Zhao, Y.H., Masuoka, T., Tsuruta, T., 2002, Unified theoretical prediction of fully developed nucleate boiling and critical heat flux based on a dynamic microlayer model. *Int. J. Heat Mass Transfer*, vol. 45, pp. 3189-3197.